Applied Water Science (2024) 14:212
https://doi.org/10.1007/s13201-024-02265-5

ORIGINAL ARTICLE

Evaluation of a solar-driven adsorption desalination system for Brazilian semiarid region

Roberto Capparelli Marçal[1] · **Mário Benjamim Baptista de Siqueira**[1]

Received: 20 December 2023 / Accepted: 4 August 2024

Abstract

In this study, the effect of using a hybrid solar thermal-activated adsorption desalination system for brackish water is evaluated under the climatic conditions of the Brazilian semiarid region. The proposed theoretical model utilizes climatic data from the meteorological station in Campina Grande, PB, and adsorptive kinetics data of Fuji Davison RD 260 silica gel to predict the performance indices of the specific daily water production (SDWP), specific cooling power (SCP), and coefficient of performance (COP) performance coefficients over a characteristic day. The SDWP value of 6.26 m3/ton, SCP ranging from 50 to 300 W/kg, and an average COP of 0.5 were obtained, considering variations in global horizontal irradiance in the ACDS system and transient ambient temperature. It was observed that both the production of desalinated water and the refrigeration effect increase with the rise in daily solar irradiance. The variation in the number of solar collectors used in the system and their optimality, as well as the variation in the salinity index of the feed source, impacted the evaluated performance coefficients.

Keywords Adsorption · Desalination · Silica gel · Solar desalination · Brackish water

Abbreviations

COP	Coefficient of performance
GOR	Gain output ratio
IDRA	International Desalination and Reuse Association
RO	Reverse osmosis
SADCS	Solar adsorption desalination cooling systems
SCP	Specific cooling power
SDWP	Specific daily water production
HDH	Humidification–dehumidification
ETC	Evacuated tube solar collector

List of Symbols

$\Delta_{isos.ads}$	Variation of isosteric enthalpy
C_m	Maximum adsorption capacity
C_p	Specific heat capacity [kJ kg^{-1} K^{-1}]
C_w	Water specific heat capacity [J kg^{-1} K^{-1}]
D_s	Surface diffusivity [m^2 s^{-1}]
D_{so}	Diffusivity [m^2 s^{-1}]
E_a	Activation energy [kJ kg^{-1}]
h_f	Fluid enthalpy [kJ kg^{-1}]
h_{fg}	Fluid gas enthalpy [kJ kg^{-1}]
K_0	Pre-exponential constant [KPa^{-1}]
K_s	Heat loss coefficient storage [W m^{-2} K^{-1}]
$\dot{m}$	Flow rate [kg s^{-1}]
R_p	Radius of silica gel particle [m]
η_o	Optical efficiency [-]
A	Area [m^2]
I_c	Global horizontal irradiance [W m^{-2}]
M	Mass [Kg]
P	Pressure [KPa]
R	Universal gas constant
T	Temperature [°C]
T	Time [s]
U_l	Overall heat transfer coefficient [W m^{-2} K^{-1}]
V	Volume [m^3]
X	Tòth isotherm constant [-]
X	Uptake [Kg.kg^{-1}]
υ_l	Outlet flow rate [m^3 s^{-1}]
χ	Concentration [ppm]
ρ	Fluid density [kg m^{-3}]

✉ Roberto Capparelli Marçal
roctb_25@hotmail.com

Mário Benjamim Baptista de Siqueira
mariosiqueira@unb.br

[1] Departamento de Engenharia Mecânica, Faculdade de Tecnologia, Universidade de Brasília–UnB, Campus Universitário Darcy Ribeiro, Asa Norte, Brasília, DF, Brazil

Published online: 05 September 2024

Subscript/superscript

ads	Adsorption
amb	Ambient
Ar	Adsorption reactor
B	Brine
C	Collector
chil w	Cooling water
cond	Condenser
evap	Evaporator
hx	Heat exchanger
In	Inlet
out	Outlet
S	Thermal reservoir
Sg	Silica gel
sw	Saline water
W	Water
υ	Flow rate
V	Vapor

Introduction

Drinking water is an essential resource for the development of agriculture, industry, and domestic activities. The growth of the world population challenges the food and goods supply. It is estimated that by the year 2030, the demand for drinking water will have increased by 2%, raising the demand to 6,900 billion m^3 (Bnm^3) per year, while the sustainable supply from the natural water cycle on the planet is 4,200 (Bnm^3) (Ng et al. 2013). In addition to the pressure of economic activities on drinking water consumption, climate change alters the balance in the rainfall regime, subjecting regions to extreme events such as floods and prolonged droughts. It is estimated that 80% of the planet's population is already experiencing water stress, which is more severe in desert and semiarid climate regions.

The scarcity of surface freshwater sources and the constant increases in the costs of collecting and treating conventional sources have been leading many countries to seek alternative solutions. A practical solution to mitigate the effects of global water scarcity lies in the development of environmentally and economically sustainable technologies for converting marine or brackish water sources into potable water by desalination, which is the process of separating excess salt and other minerals from saline water. According to the report published by IDRA (International Desalination and Reuse Association 2019) the most widely used desalination technologies are thermally activated processes like multi-stage-flashing (MSF) and multi-effect distillation (MED), with 27 and 9% participation in the global installed capacity, respectively, and electrical energy triggered processes such as reverse osmosis (RO), electro-dialysis (ED), and vapor compression (VC), responsible for 59, 4, and 1% of the global capacity, respectively. All these existing desalination technologies have limitations regarding their use, especially high maintenance costs and high energy consumption, between 2.5 and 12 kWh/m^3. Furthermore, it is observed that, in general, regions with poor drinking water supplies also have problems with electricity.

Such a scenario is a reality in the semiarid region of Northeast Brazil, where the scarcity of surface water resources has driven the search for groundwater sources. However, due to the geological formation of crystalline rock, most drilled wells in this region exhibit salinity levels higher than recommended by health authorities. The Brazilian Federal Government, through the "Água Doce" program (Brazil 2010; Ferreira et al. 2017), has promoted the installation of desalination plants based on RO technology. This process is entirely dependent on the availability and quality of an electrical power supply, which may not always be accessible to the most remote communities. Consequently, researchers and engineers are confronted with the task of exploring alternative desalination processes or systems capable of utilizing alternative energy sources, featuring low operating costs, and minimizing environmental impact.

One process that meets these requirements is adsorption desalination activated by thermal solar energy. This process is based on the characteristics of vapor (adsorbate) adsorption by the surface of certain porous media, such as, in this case, silica gel (adsorbent). The adherence of adsorbate molecules to the surface of the adsorbent is a physical process that occurs due to weak van der Waals electrostatic forces and can be completely reversed by altering the temperature and pressure conditions. Desalination based on the adsorption process, thermally activated, was introduced by Ng et al. (2013) as an emerging process that is energy-efficient and environmentally friendly.

Additionally, adsorption desalination provides a cooling effect that can be utilized for food and goods refrigeration, offering an additional benefit at no extra cost. It is worth mentioning other competitive advantages when compared to other conventional processes: (a) low maintenance costs due to the absence of moving parts; (b) environmental sustainability due to the non-use of chemical products; (c) lower incidence of evaporator scale due to operation at low evaporating temperatures; and (d) can be activated by low-intensity thermal sources such as non-concentrated solar energy or residual heat from industrial processes.

Therefore, it is not surprising that the topic of desalination by adsorption has attracted growing interest from various authors in recent years, as seen in Ng et al. (2009, 2012, 2013), Wu et al. (2010), Youssef et al. (2016), and Alsaman et al. (2017), just to cite a few studies in the literature. In these studies, authors commonly reach a consensus by utilizing specific performance indices like SDWP (specific daily water production), SCP (specific cooling power),

and COP (coefficient of performance) to assess and compare their results with those found in the existing literature. The adoption of these indices enables the comparison of systems with diverse configurations. In order to maximize these performance indicators, various authors propose new arrangements for the adsorption desalination system (Thu et al. 2013a; Li et al. 2021), define new operational strategies (Thu et al. 2009), altering the input parameters such as temperatures of the thermal source and cooling (reactor and condenser) (Youssef et al. 2015a) and variations in flow rates, and cycle time (Alsaman et al. 2017; Rezk et al. 2019; Askalany et al. 2021). Other authors propose performance evaluations of ACDS systems based on the use of new adsorbent materials and new compounds such as silica gel (Ng et al. 2001, 2013; Wu et al. 2012; Thu et al. 2013b; Alsaman et al. 2017), zeolites (Myat et al. 2013; Goldsworthy 2014; Youssef et al. 2015b; Ali and Chakraborty 2016; Wibowo et al. 2017; Liu et al. 2021), and MOFs (Elsayed et al. 2017; Elsayed et al. 2020; Han and Chakraborty 2022) Other studies aiming to improve heat transfer in adsorptive reactors propose advanced design heat exchangers such as Alam et al. (2000); Vivekh et al. (2018); Velte-Schäfer et al. (2023) and Gado et al. (2024).

All these previous studies currently favor the expansion of possibilities for proposing new systems through the hybridization of these strategies, incorporating the technological improvements achieved, as demonstrated in the most recent works presented by Ali et al. (2024a, b), who studied the hybridization of adsorption processes with humidification–dehumidification (HDH) systems. They investigated solar-powered adsorption desalination systems using composite sodium polyacrylate (SP) as the adsorbent, integrated with HDH systems driven by solar energy or waste heat. In this study, the authors also included a cost analysis and assessed the impact of weather on performance. The results showed a value of 77.3 m^3/ton for the SDWP, with costs of \$1.83/m^3 for solar energy-based systems and \$0.49/m^3 when evaluated with waste heat.

In another similar study, Ali et al.(2024b), four innovative configurations are proposed and compared to enhance water productivity and energy utilization. The maximum water production achieved was between 1.7 and 3 m^3/day at 120 °C. The highest gain output ratio (GOR) observed ranged from 1.49 to 1.69 at 120 °C. The proposed integrations show remarkable energy utilization efficiency, particularly with low-temperature heat sources (55–65 °C).

In Alsaman et al. (2024), the authors explore innovative configurations of hybrid adsorption desalination combined with a humidification–dehumidification system, utilizing solar energy or waste heat across four different operational modes. The study includes an economic cost analysis and evaluates system performance using raw silica gel and silica gel/$CaCl_2$ adsorbents, based on weather conditions in Assiut, Egypt. The results indicated that, in June, the cost of freshwater production was \$2/m^3, with the SDWP and GOR achieving values of 1.8 and 69 m^3/ton, respectively.

However, only a few researchers have examined how changing climatic conditions and variations in the saline concentration of the brackish water feed source impact the performance indexes of solar-powered adsorption desalination systems. In Olkis et al. (2021), a comparative experimental study, assessments were made regarding the variation in solar radiation in Scotland and Sicily (Italy) on the performance of the solar-powered adsorption desalination system. For Scotland, the system was found to be viable only during the summer and spring seasons, while in Sicily, it proved to be feasible throughout the year, achieving an SDWP of 7.14 m^3/ton of adsorbent from 200 m^2 of solar collectors. In a similar study, (Ali et al. 2017; Pakere et al. 2018) evaluate the application of a hybrid desalination and cooling system powered by solar energy under the climatic conditions of Egypt. In the theoretical model proposed by the authors, the system includes temperature control devices for the thermal source, operating at a minimum of 85 °C, and the performance indicators achieved for SDWP are a maximum of 10 m^3/ton, COP of 0.5, and SCP of 134 W/kg. In another study, Bai et al. (2020) propose a theoretical and experimental model for assessing the performance of a solar thermal-activated adsorption desalination system subjected to a temperature of 85 °C, an evaporator temperature of 14 °C, and a cycle time of 19 min. The authors evaluate the indices as a function of the variation in various inputs, including the salinity index of the feed source. For seawater with an average salinity of 35 g/kg, an SDWP of 18 m^3/ton and an SCP of 490 W/kg were achieved; however, for increasing salinity values, the SDWP decreases.

Although the recent studies mentioned above have revealed promising results for the desalination process of seawater in coastal regions, these studies mostly rely on the evaluation of adsorptive cycles with preset operational parameters such as temperatures of the thermal source and cooling, saline concentration of the feed source, and cycle time. These systems, despite being able to be activated by waste heat or other low-intensity heat sources, are not independent of electricity consumption, which is necessary for the operation of recirculation pumps, vacuum pumps, and any control and automation systems. For the operation of this system in remote areas not served by the electrical grid, alternative systems for thermal and electrical energy generation should be considered.

The contribution of this work lies in the evaluation of performance in terms of SDWP, SCP, and COP of a simplified, small-scale, and low-cost adsorption-based desalination and cooling system activated by solar thermal energy. The proposed system and model are evaluated for application in the desalination processes of brackish water typical

of underground wells in the semiarid climate region of northeastern Brazil. To achieve this, a new representative numerical lumped model is proposed, simulating a typical adsorption desalination system composed of an evaporator, condenser, and dual thermally activated reactor powered by solar collectors operating completely off the electrical grid. The input parameters adopted for the simulation of the model take into account the daily variations in meteorological conditions, such as ambient temperature and solar irradiation levels, with their respective impacts on the adsorptive cycle temperatures. Unlike various studies presented in the literature, where the performance indices of ADCS systems are evaluated according to pre-adjusted parameters, the innovation of this lumped model lies in its ability to simultaneously evaluate the performance indices, SDWP, SCP, and COP, by considering the temperature transients caused by changes in climatic conditions and the seasonality of the salinity levels of the source throughout a characteristic day. A brief discussion on the applicability of this technology as an alternative to the current reverse osmosis (RO) desalination processes used in this region is also presented.

Materials and methods

Description of the proposed desalination system (SACDS)

The proposed desalinator system comprises three primary components: the adsorptive reactors (using silica gel as an adsorbent), the condenser, and the evaporator. In this setup, the desalination system operates intermittently, with the reactors functioning alternately during the adsorption and desorption cycles. The system is thermally activated by evacuated tube solar collectors (ETC). Figure 1 schematically illustrates the system, naming its components.

Operationally, the system works as follows: After evacuation of the entire system and having loaded and degassed the saline water tank, the valve between the evaporator (19, in Fig. 1) and the saltwater reservoir (16, in Fig. 1) is then opened. Consequently, the saline water evaporates and feeds the adsorptive reactor (2, in Fig. 1) with its vapor through the opening of the valve between the evaporator and the reactor. The silica gel bed (3, in Fig. 1) adsorbs the water steam, and the generated heat is evacuated by circulating cooling water in the reactor. Once the adsorptive bed is saturated, the valve between the evaporator and the reactor is closed, and the one between the reactor (1, in Fig. 1) and the condenser (7, in Fig. 1) is opened.

Hence, the hot water recirculation system from the solar panel (23, in Fig. 1) replaces the cooling water recirculation system. An increase in temperature in the adsorptive bed leads to the extraction of steam from the adsorbed water, which regenerates the silica gel. Following the opening of the valve between the reactor and the condenser, the steam condenses and fresh water is collected.

Once the temperature of the adsorptive bed reaches its maximum, the regeneration process of the silica gel is completed, making the system ready to initiate another cycle. It is worth mentioning that saline or brackish water is distilled twice, and one can benefit from the cooling effect formed in the evaporator either in a refrigeration system or also in the cooling system of the condenser and adsorptive reactor. One more advantage of the adsorption desalination system is its

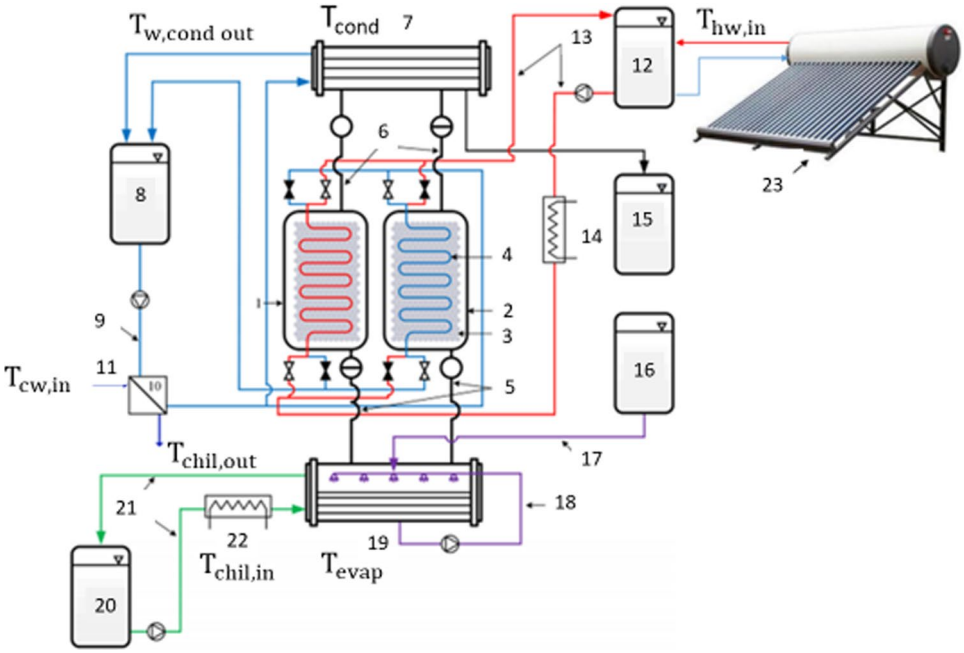

Fig.1 Schematic diagram of SACDS: 1, 2: reactor vessel; 3: adsorbent material; 4: finned radiator; 5, 6: steam piping; 7: condenser; 8: cold water reservoir; 9: cold water piping; 10: thermal exchanger; 11: cold water return piping; 12 thermal water source; 13: thermal water piping; 14: heat exchanger; 15: potable water collector; 16: degassed saltwater reservoir; 17: saltwater feed piping; 18: saltwater recirculation piping; 19: evaporator; 20: cooled water reservoir; 21: cooled water piping; 22: heat exchanger; and 23: solar thermal collector

flexibility; in fact, it can be configured to obtain bi-distilled drinking water or both bi-distilled water and chilled water.

Thermodynamically, the processes can be conveniently described in a P–T-X diagram, where P is pressure, T is temperature and X stands for the amount of adsorbed by the adsorbent (kg/kg) under equilibrium conditions. Figure 2 illustrates the theoretical P–T-X diagram of an adsorption cycle, and this cycle presents 4 processes; two isosteric and two isobaric:

- **Process 1–2**-Starting the process at point 1, following the closure of the valve between the bed and the evaporator, the recirculation of the cooling water is interrupted and that of the hot water is increased in the adsorptive reactor; consequently, the temperature and the pressure of the hot water increase along the constant concentration line $X_{max} = X_1 = X_2$. The later process continues until the saturation pressure at the condenser temperature is reached, point 2.
- **Process 2–3**-At point 2, the opening of the valve between the adsorptive reactor and the condenser leads to transfer of the desorbed vapor from the silica gel bed to the condenser. Following the recirculation of cooling water through the condenser, water vapor gets condensed. The pressure in the condenser as well as in the adsorptive reactor remains constant until the temperature in the adsorption bed reaches its maximum and the concentration $X_{min} = X_3 = X_4$.
- **Process 3–4**-At point 3, the temperature in the adsorptive bed reaches its highest value. At this point, due to the closure of the valves, the reactor is isolated from the condenser and the evaporator. Then, the water recirculation process begins, and the bed temperature decreases along the constant concentration line X_{min} until reaching point 4 where the pressure P_4 is the vapor saturation pressure at the evaporator temperature.
- **Process 4–1**-In the final stage starting at point 4, the opening of the valve between the adsorptive reactor and the evaporator makes the cooling water recirculating through the adsorptive bed. The amount of saline water fed into the evaporator starts to evaporate, and the vapor is transferred to the adsorptive reactor due to the valve opening. During this process, the pressure remains constant $P_4 = P_1$, while the temperature of silica gel bed continues to decrease until reaching T_1 that is determined by the temperature of the cooling water. At point 1, the concentration of water in the silica gel bed is at its maximum $X_1 = X_{max.}$

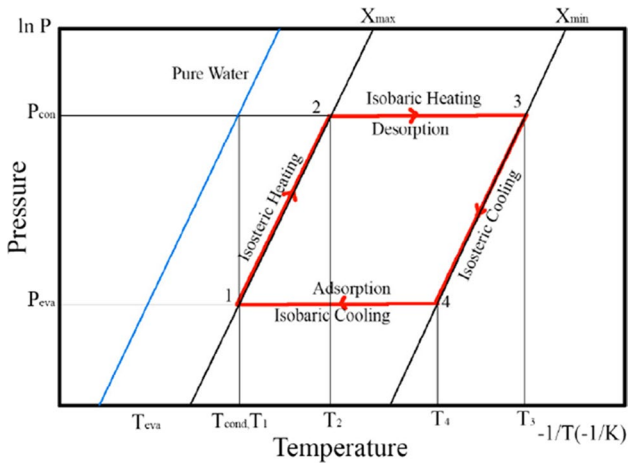

Fig.2 Adsorption desalination cycle diagram

Mathematical modeling

This section describes the development of a lumped mathematical model applied to a solar desalination system based on an adsorption cycle (SACDS) carried out by an apparatus composed of two subsystems. The first subsystem is composed of solar collectors and the thermal reservoir, which are responsible for supplying the thermal energy necessary to carry out the adsorptive cycle. The second subsystem is composed of the adsorptive reactors containing the heat exchangers loaded with the adsorbent material (Silica-gel RD 2560) coupled to an evaporator and a condenser. The definition of the differential equations that make up the SADCS model is based on the application, in each component of the system, of the thermodynamic concept of mass and energy conservation, as well as the analysis of the isotherms of the adsorptive kinetics of the silica gel–water pair. The aim of proposing a representative mathematical model for a SADCS system is to enable the simulation of the system's performance when subjected to changes in various operational parameters and variations in climatic conditions. To facilitate the development and mathematical solution of the model, several considerations are listed: (i) the adsorptive reactors, the evaporator, and the condenser are evaluated as a compact set, not considering variations in temperature and pressure between them; (ii) the temperature and pressure, as well as the diffusion of vapor in the adsorbent bed, are considered homogeneous for the adsorptive reactors; (iii) it is assumed that the adsorbed water vapor behaves like water in the saturated liquid state; therefore, properties such as density and specific heat are evaluated considering this thermodynamic condition; (iv) the pressure drop due to steam and water flow in the circuit is disregarded; (v) due to good thermal insulation, heat losses through the surfaces of adsorptive reactors, evaporator, condenser, and piping are disregarded; (vi) vapor density is significantly lower than silica gel and water; therefore, its thermal capacity is not taken into account; (vii) both the gas phase adsorbate (water vapor) and the adsorbent

(silica gel) are in equilibrium; and (viii) the temperature and pressure in the reservoir and solar collector are considered homogeneous.

These considerations may be reasonable as they simplify the model and are justified by the fact that the system features small-scale components and their tubing, which are thermally well-insulated. Additionally, the system operates with extended cycles, reducing the effects of thermal resistance between the adsorbent material and the heat exchanger, as well as the effects of vapor diffusion within the porous medium.

Adsorptive system

Initially, to estimate the amount of adsorbed vapor, it is necessary to evaluate the characteristic adsorption isotherms of the adsorbent material under different values of temperature and pressure. Under a specific equilibrium condition, at a pressure (P) and temperature (T), this quantity can be determined by the Tòth isotherm model (Chua et al. 2002a; Mitra et al. 2017) below:

$$C^* = \frac{K_0.\exp\left(\frac{\Delta h_{\text{isos,ads}}}{RT}\right).P}{\left[1+\left\{\left(\frac{K_0}{C_\text{m}}\right)\exp\left(\frac{\Delta h_{\text{isos,ads}}}{RT}\right).P\right\}^x\right]^{\frac{1}{x}}} \tag{1}$$

where C^* is the vapor uptake by the mass of adsorbent in the equilibrium condition and on the right side of the equation; K_o is the pre-exponential constant, $\Delta h_{\text{isos,ads}}$ is the variation of the isosteric enthalpy during the adsorption process, x is the dimensionless Tóth parameter, C_m is the maximum uptake capacity of the adsorbent material, and R is the characteristics gas constant. The vapor capture is transient at a given pressure and temperature; that is, the adsorption and desorption kinetics are modeled using the equation of the linear driving force (LDF) model given by (Chihara and Suzuki 1983; Sakoda and Suzuki 1984):

$$\frac{dC(t)}{dt} = K_\text{s}a_\text{p}.(C^* - C(t)) \tag{2}$$

where $K_\text{s}.a_\text{p}$ is the overall mass transfer coefficient for the adsorption process operating in low-pressure regimes (2–10 kPa) expressed in terms of the parameters R_p and D_so. The adsorption rate is controlled by surface diffusion inside a particle, and the surface diffusivity D_s is given as a function of temperature (Chihara and Suzuki 1983; Sakoda and Suzuki 1984):

$$K_\text{s}a_\text{p} = 15.\frac{D_\text{s}}{R_\text{p}^2} \tag{3}$$

$$D_\text{s} = D_\text{so}\exp\left(-\frac{E_\text{a}}{RT}\right) \tag{4}$$

The parameters indicated in expressions (3) and (4) denote; R_p the mean radius of the silica gel grain, D_so the kinetic constant of the silica gel and water system, and E_a the activation energy. The value of D_so and E_a in this study is obtained from (Aristov et al. 2006). The application of mass conservation for the salt concentration in the evaporator of an adsorption desalination cooling cycle (ADC) takes into account the quantities referring to the mass flow of the saltwater feed (seawater or brackish), the mass production of drinking water extracted from the condenser, and the disposal rate of the tailings concentrated in the form of brine. This mass balance, therefore, is represented by the following equation (Ng et al. 2013; Alsaman et al. 2017):

$$\frac{\text{d}M_{\text{sw,evap}}}{\text{d}t} = \theta.\dot{m}_{\text{sw,in}} - \eta.\left(\frac{\text{d}C_{\text{ads}}}{\text{d}t}\right).M_{\text{sg}} - \gamma.\dot{m}_\text{b} \tag{5}$$

where C_{ads} denotes the vapor uptake by the adsorbent material in the adsorption process and is obtained from Eq. (1). The coefficients, θ, η, and γ, are operational parameters and are applied to the model to fit the cycle phase and the values adopted are presented in the next section in Table 1. $M_{\text{sw,evap}}$ is the amount of brackish or seawater contained in the evaporator, $\dot{m}_{\text{sw,in}}$ is the mass flow of saltwater feeding into the evaporator, and $\dot{m}_\text{b}$ is the extraction rate of concentrated brine from the evaporator. This extraction occurs when the saline concentration inside the evaporator reaches a preset value. The saline water is pumped intermittently to the evaporator, depending on the volume and level adjustment. The mass balance Eq. (5) in the evaporator can be rewritten in terms of the salt concentration balance in the ADC system (Ng et al. 2013; Alsaman et al. 2017):

$$\begin{aligned} M_{\text{sw,evap}}\frac{\text{d}\chi_{\text{sw,evap}}}{\text{d}t} &= \theta.\chi_{\text{sw,in}} \\ &.\dot{m}_{\text{sw,in}} - \eta.\chi_v.\left(\frac{\text{d}C_{\text{ads}}}{\text{d}t}\right).M_{\text{sg}} - \gamma.\chi_{\text{sw,evap}}.\dot{m}_\text{b} \end{aligned} \tag{6}$$

In this equation, $\chi_{\text{sw,in}}$ denotes the saline concentration of saltwater (brackish or seawater) pumped to the evaporator, χ_v the steam concentration in the evaporator at equilibrium condition and $\chi_{\text{sw,evap}}$ the salt concentration in the evaporator. Applying the concept of energy balance to the evaporator yields the following equation (Ng et al. 2013; Alsaman et al. 2017):

Table 1 Operational parameters

Mode	Parameter	2-bed reactor
Operation	η	2
	θ	1 (feeding saline water)
		0 (otherwise)
	γ	1 (brine discharge)
		0 (otherwise)
Switching	η	2
	θ	1 (feeding saline water)
		0 (otherwise)
	γ	1 (brine discharge)
		0 (otherwise)

$$\begin{aligned}&\left[M_{\mathrm{sw,evap}}.C_{\mathrm{p,sw}}\left(T_{\mathrm{evap}},\chi_{\mathrm{sw,evap}},P_{\mathrm{evap}}\right)+M_{hx,\mathrm{evap}}.C_{\mathrm{p,hx,\ evap}}\right]\frac{\mathrm{d}T_{\mathrm{evap}}}{\mathrm{d}t}\\&=\theta.h_{\mathrm{f,sw}}\left(T_{\mathrm{evap}},\chi_{\mathrm{sw,evap}},P_{\mathrm{evap}}\right)\\&\quad.\dot{m}_{\mathrm{sw,in}}-\gamma.h_{\mathrm{f,b}}\left(T_{\mathrm{evap}},\chi_{\mathrm{sw,evap}},P_{\mathrm{evap}}\right)\\&\quad.\dot{m}_{\mathrm{b}}-\eta.h_{\mathrm{fg}}\left(T_{\mathrm{evap}}\right)\frac{\mathrm{d}C_{\mathrm{ads}}}{\mathrm{d}t}\\&\quad.M_{\mathrm{sg}}+\dot{m}_{\mathrm{chil\ w}}.C_{\mathrm{p,chil\ w}}\left(T_{\mathrm{evap}}\right).\left(T_{\mathrm{chil\ w,in}}-T_{\mathrm{chil\ w,out}}\right)\end{aligned}\tag{7}$$

where $M_{hx,\mathrm{evap}}$ is the total evaporator mass, M_{sg} is the total mass of the silica gel adsorbent, and $\dot{m}_{\mathrm{b}}$ is the mass flow rate of the concentrated brine discharge. The first term on the right side of Eq. (7) represents the amount of sensible heat added to the system due to the supply of saline water to the evaporator, the second one refers to sensible heat due to brine discharge, the third term denotes the amount of heat removed in the adsorption process, and the fourth refers to the amount of heat provided by the cooling water stream feed. The parameters $C_{\mathrm{p,sw}}$, sensible heat, and the enthalpies $h_{\mathrm{f,b}}$ and $h_{\mathrm{f,sw}}$ of saline water are calculated through correlations as a function of temperature, salt concentration, and pressure (Nayar et al. 2016).

The estimated outlet temperature of the cooling water in the evaporator $T_{\mathrm{chil\ w,out}}$ is determined through the application of the logarithmic mean temperature difference method as described by Eq. (8) (Kakaç et al. 2012).

$$T_{\mathrm{chil\ w,out}}=T_{\mathrm{evap}}+\left(T_{\mathrm{chil\ w,in}}-T_{\mathrm{evap}}\right)\exp\left\{\frac{-U.\mathrm{A}_{\mathrm{evap}}}{\dot{m}_{\mathrm{chil\ w}}.C_{\mathrm{p,chil\ w}}}\right\}\tag{8}$$

where the term $U.A_{\mathrm{evap}}$ denotes the overall heat transfer coefficient of the evaporator. The energy balance for the condenser coupled to the adsorptive reactors can be evaluated through the following relationship:

$$\begin{aligned}&\left[M_{\mathrm{w,cond}}.C_{\mathrm{p_{w\ cond}}}\left(T_{\mathrm{cond}}\right)+M_{\mathrm{hx,cond}}.C_{\mathrm{p_{hx,\ cond}}}\right]\frac{\mathrm{d}T_{\mathrm{cond}}}{\mathrm{d}t}\\&=-h_{\mathrm{f}}\left(T_{\mathrm{cond}}\right)\frac{\mathrm{d}M_{\mathrm{wd}}}{\mathrm{d}t}+\eta.h_{\mathrm{fg}}\left(T_{\mathrm{cond}}\right)\frac{dC_{\mathrm{des}}}{dt}.M_{\mathrm{sg}}\\&\quad+\dot{m}_{\mathrm{w\ cond}}.C_{\mathrm{p_{w\ cond}}}T_{\mathrm{cond}}\right).\left(T_{\mathrm{w\ cond,\ in}}-T_{\mathrm{w\ cond\ ,out}}\right)\end{aligned}\tag{9}$$

where $M_{\mathrm{w\ cond}}$ is the mass of steam condensed in the condenser, M_{wd} the quantity of distilled water obtained in the condenser, $h_{\mathrm{fg\ (Tcond)}}$ denotes the enthalpy of steam saturation evaluated at the condenser temperature, and $\dot{m}_{\mathrm{w\ cond}}$ is the mass flow rate of cooling water in the condenser at the inlet temperature $T_{\mathrm{w\ cond,\ in}}$ and the outlet temperature $T_{\mathrm{w\ cond,out}}$. Likewise, the estimated outlet temperature for the cooling water in the evaporator $T_{\mathrm{w\ cond,out}}$ is determined by applying the logarithmic mean temperature difference method, as outlined in Eq. (10) (Kakaç et al. 2012).

$$T_{\mathrm{w\ cond,out}}=T_{\mathrm{cond}}+\left(T_{\mathrm{w\ cond,in}}-T_{\mathrm{cond}}\right)\exp\left\{\frac{-U.A_{\mathrm{cond}}}{\dot{m}_{\mathrm{w\ cond}}.C_{\mathrm{p_{w\ cond}}}}\right\}\tag{10}$$

where $U.A_{\mathrm{cond}}$ is the overall heat transfer coefficient in the condenser. The energy balance equation for the adsorptive bed reactor that contains the silica gel mass and the finned heat exchanger, which is also coupled to the evaporator and condenser, is given by the expression:

$$\begin{aligned}&\left[M_{\mathrm{sg}}.C_{\mathrm{p_{\ sg}}}+M_{\mathrm{hx,bed}}.C_{\mathrm{p_{\ hx,bed}}}+M_{\mathrm{sg}}.C_{\mathrm{p_o}}.C^{*}\right]\frac{\mathrm{d}T_{\mathrm{ads/des}}}{\mathrm{d}t}\\&=\pm\eta.\Delta h_{\mathrm{isos,\ ads/des}}(T_{\mathrm{ads/des}},P_{\mathrm{ads/des}})\\&\quad.M_{\mathrm{sg}}\frac{\mathrm{d}C_{\mathrm{ads/des}}}{\mathrm{dt}}\pm\dot{m}_{\mathrm{h/c\ w}}.C_{\mathrm{p_{\ h/c\ w}}}\left(T_{\mathrm{h/cw}}\right)\\&\quad.(T_{\mathrm{h/cw\ in}}-T_{\mathrm{h/cw\ out}})\end{aligned}\tag{11}$$

The terms presented on the left side of the equality above represent the sensible heat of the heat exchanger set of the adsorptive bed where the specific heat of the silica gel, the mass of the metallic components, and the mass of the adsorbent modeled as liquid phase are taken into account. The first term on the right side denotes the enthalpy variation during the adsorption and desorption processes that occur inside the adsorptive bed. The parameter $\Delta\mathrm{h}_{\mathrm{isos,ads/des}}$ ($T_{\mathrm{ads/des}}$, $P_{\mathrm{ads/des}}$) is called isosteric heat and quantifies the heat supplied or rejected in the adsorptive bed during the adsorption and desorption processes (Ruthven 2008; Alsaman et al. 2017).

The term, $T_{\mathrm{h/cw\ out}}$, represents the outlet temperatures of the water used in the heating and cooling steps of the adsorptive reactor heat exchanger during the adsorption and desorption. $T_{\mathrm{h/cw\ out}}$ can be assessed by employing a similar approach to the other heat exchangers in the model, the logarithmic mean temperature method (LMTD) as:

$$T_{\mathrm{h/c\ w,out}} = T_{ar} + \left(T_{\mathrm{h/c\ w,\ in}} - T_{ar}\right)\exp\left\{\frac{-U.A_{\mathrm{ar}}}{\dot{m}_{\mathrm{h/c\ w}}.C_{\mathrm{p_{h/c\ w}}}}\right\} \tag{12}$$

where $U.A_{\mathrm{ar}}$ is the overall heat transfer coefficient in the adsorptive reactor. The numerical solution of the ordinary differential Eqs. (2), (5), (6), (7), (9), and (11) constitutes the model to describe the evolution of daily potable water production to be used here. Numerical models experimentally validated for the adsorption subsystem and similar to the model proposed here are presented by various authors in the literature such as Mitra et al. (2014), Youssef et al. (2016) and Alsaman et al. (2017).

Mathematical modeling of the solar collector and thermal storage system

Next, the two Eqs. (13) and (14) represent the mathematical model that describes the temperature transient process in the collector (T_{c}) and reservoir (T_{s}). These equations are obtained from the energy balance applied to the solar collector and thermal reservoir, considering that the temperature of the thermal fluid in the collector and the reservoir is thermally mixed. This model proposed by Buzás et al. (1998) and Buzás (2009), despite its simplicity, provides satisfactory solutions with good accuracy. This can be confirmed in other works available in the literature as in the models presented and validated by Kicsiny and Varga (2012) and Kumar and Rosen (2010). Figure 3 schematically shows the modeled subsystem.

$$\frac{\mathrm{d}T_{\mathrm{c}}}{\mathrm{d}t} = \frac{A_{\mathrm{c}}.\eta_{\mathrm{o}}}{\rho.c_{\mathrm{w}}.V_{\mathrm{c}}}.I_{\mathrm{c}} + \frac{U_{\mathrm{l}}.A_{\mathrm{c}}.(T_{\mathrm{amb}} - T_{\mathrm{c}})}{\rho.c_{\mathrm{w}}.V_{\mathrm{c}}} + \frac{\nu.(T_{\mathrm{s}} - T_{\mathrm{c}})}{V_{\mathrm{c}}} \tag{13}$$

$$\frac{\mathrm{d}T_{\mathrm{s}}}{\mathrm{d}t} = \frac{\nu.(T_{\mathrm{c}} - T_{\mathrm{s}})}{V_{\mathrm{s}}} + \frac{\nu_{\mathrm{l}}.(T_{\mathrm{cold}} - T_{\mathrm{s}})}{V_{\mathrm{s}}} + \frac{A_{\mathrm{s}}.K_{\mathrm{s}}.(T_{\mathrm{amb}} - T_{\mathrm{s}})}{\rho.c_{\mathrm{w}}.V_{\mathrm{s}}} \tag{14}$$

Equations (16) and (17), along with the adsorption cycle model described above, establish a comprehensive model for estimating the performance indices of the desalination system, given the input values of I_{c}, T_{amb},$\chi_{\mathrm{sw,in}}$.

Performance indicators

To evaluate the adsorption cycle, Specific Water Production (SWP), which measures the amount of distilled water produced per amount of adsorbent per cycle, is used. Since the refrigeration effect is also intended to be used, two other parameters are used to assess the performance of the cycle: specific cooling power (SCP) and coefficient of performance (COP). These parameters are calculated using the equations:

$$\mathrm{SWP} = \int_0^{t_{\mathrm{cycle}}} \frac{\dot{m}_{\mathrm{w\ cond}}.C_{\mathrm{p_{w\ cond}}}\left(T_{\mathrm{cond}}\right).\left(T_{\mathrm{w\ cond,out}} - T_{\mathrm{w\ cond\ ,\ in}}\right)}{h_{\mathrm{fg}}\left(T_{\mathrm{cond}}\right).M_{\mathrm{sg}}}\mathrm{d}t \tag{15}$$

$$\mathrm{SCP} = \int_0^{t_{\mathrm{cycle}}} \frac{\dot{m}_{\mathrm{chil\ w}}.C_{\mathrm{p_{chil\ w}}}\left(T_{\mathrm{chil}}\right).\left(T_{\mathrm{chil,\ in}} - T_{\mathrm{chil,out}}\right)}{M_{\mathrm{sg}}}\mathrm{d}t \tag{16}$$

$$\mathrm{COP} = \int_0^{t_{\mathrm{cycle}}} \frac{\dot{m}_{\mathrm{chil\ w}}.C_{\mathrm{p_{chil\ w}}}\left(T_{\mathrm{chil}}\right).\left(T_{\mathrm{chil,\ in}} - T_{\mathrm{chil,out}}\right)}{\dot{m}_{\mathrm{h\ w}}.C_{\mathrm{p_{h\ w}}}\left(T_{\mathrm{h\ w}}\right).\left(T_{\mathrm{h\ w,\ in}} - T_{\mathrm{h\ w,out}}\right)}\mathrm{d}t \tag{17}$$

Additionally, the specific daily water production (SDWP) for the meteorological conditions typical in the semiarid region in Brazil is estimated.

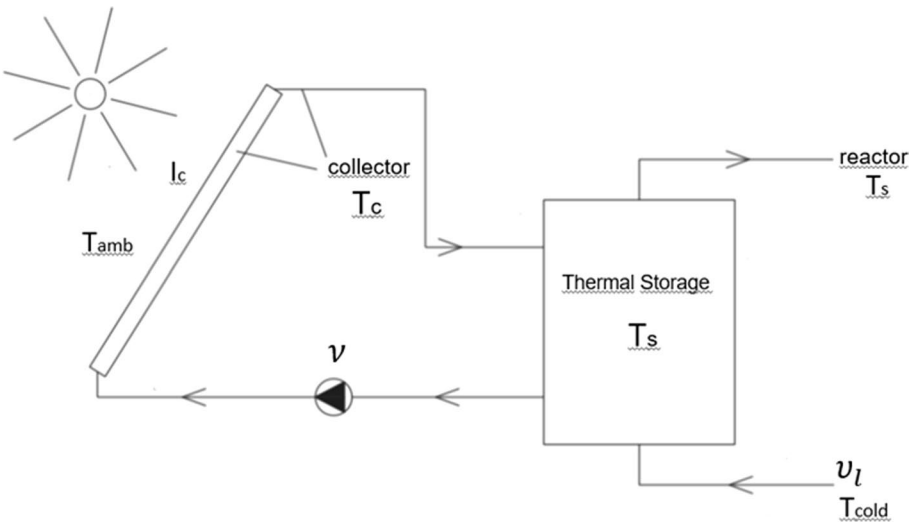

Fig.3 Thermal source solar heating

Results and discussion

Numerical simulation results

The numerical model is solved utilizing the MATLAB software coupled with the REFPROP (Reference Fluid Thermodynamic and Transport Properties Database) platform for thermophysical property data. The system of variables is solved through numerical integration of the differential equations of the model, employing the fourth-order Runge–Kutta–Felberg method with a relative error tolerance of 1.10^{-6} The parameters η, θ, and γ are used to adjust the expression according to the mode of operation of the adsorptive cycle following Table 1.

Table 2, Table 3, Table 4 provide the properties of the materials, constants, dimensional parameters, and operational variables employed in the numerical simulation for the adsorptive system, solar collector, and thermal storage models, respectively.

The thermophysical properties of the adsorbent medium utilized in this simulation were acquired based on the characteristics of the Fuji Davison RD 2560 silica gel, which is a commonly employed adsorbent by commercial chiller manufacturers. Experimental studies validating the adsorption kinetics characteristics between the silica gel and the water employed in this simulation are reported in Chua et al. (2002b) and Thu et al. (2013b). Figures 4 and 5 depict the isotherms corresponding to the adsorption and desorption processes, respectively, as a result of the model simulation

Table 2 Parameters used in numerical simulation (Chua et al. 2002a; Alsaman et al. 2017; Mitra et al. 2017)

Symbol	Description	Value	Unit
C_m	maximum adsorption capacity	0.45	kg/kg
$C_{p\,sg}$	specific heat silica gel	$0.924.10^3$	J/kg.k
$C_{p,hx\ evap}$	specific heat evaporator material/copper (Cu)	$0.386.10^3$	J/kg.K
$C_{phx,cond}$	specific heat condenser material/copper (Cu)	$0.386.10^3$	J/kg.K
$C_{phx.bed}$	specific heat exchanger material/copper (Cu)	$0.386.10^3$	J/kg.K
C_{pv}	specific heat water vapor phase	$1.89.10^3$	J/kg.K
C_{pw}	specific heat water liquid phase	$4.18.10^3$	J/kg.K
D_{so}	adsorption kinetic constant	$2.9.10^{-4}$	m^2/s
E_a	activation energy	$2.3.10^3$	kJ/kg
K_0	pre-exponential constant	$7.3.10^{-10}$	1/kPa
$M_{hx\ bed}$	mass of adsorptive reactor material	15	kg
$M_{hx,evap}$	heat exchanger material mass	1.3	kg
$M_{s,evap}$	initial mass of saline water	3	kg
M_{sg}	total silica gel mass in the reactor	7	kg
R_p	average radius of the adsorbent particle (silica gel)	$0.8.10^{-3}$	m
UA_{ar}	overall heat transfer coefficient adsorptive reactor	600	W/K
UA_{cond}	overall heat transfer coefficient condenser	500	W/K
UA_{evap}	overall heat transfer coefficient evaporator	350	W/K
$\Delta h_{isos/ads}$	isosteric enthalpy variation adsorption/desorption	2693	kJ/kg
R	universal gas constant	0.461	kJ/kg.K
x	Tòth heterogeneity constant	12	–

Table 3 Operational parameters

Symbol	Description	Value	Unit
$\dot{m}_{chil\ w}$	flow rate chilling water evaporator	0.025	kg/s
$\dot{m}_{h/cw}$	flow rate adsorptive reactor heat and cooling	0.6	kg/s
$\dot{m}_{w,cond}$	flow rate cooling water condenser	0.6	kg/s
$T_{chil,in}$	Inlet temperature, chilling water in the evaporator	20–35	°C
$T_{cw,in}$	Inlet temperature, cooling water in the adsorption reactor	20–35	°C
$T_{hw,in}$	temperature of the thermal source	20–85	°C
$T_{wcond,\ in}$	Inlet temperature, cooling water in the condenser	20–35	°C
$\chi_{sw,evap}$	pre-determined concentration of brine for tailings	50,000	ppm
$\chi_{sw,i}$	initial concentration of saline water	1000	ppm

Table 4 Parameters of the numerical simulation of the solar collector and thermal storage system

Symbol	Description	Value	Unit
A_c	collector surface area	4.461	m^2
A_s	storage surface area	2.305	m^2
I_c	global horizontal irradiance on the collector surface	0–800	W/m^2
K_s	heat loss coefficient of the storage	7.2	$W/m^2.K$
T_{amb}	environment temperature	15–35	°C
T_c	fluid temperature at the collector outlet	20–100	°C
T_{cold}	cold inlet fluid temperature of the storage/collector	20–80	°C
T_s	fluid temperature in the reservoir	20–80	°C
U_l	overall heat transfer coefficient	4.4	$W/m^2.K$
V_s	storage volume	0.268	m^3
η_o	optical efficiency of the collector	0.68	–
ν_l	outlet flow rate	6.010^{-4}	m^3/s
c	fluid specific heat capacity	4200	J/Kg.K
t	time	3,600	s
ν	collector flow rate	$3.4.10^{-5}$	m^3/s
ρ	fluid density	1000	Kg/m^3

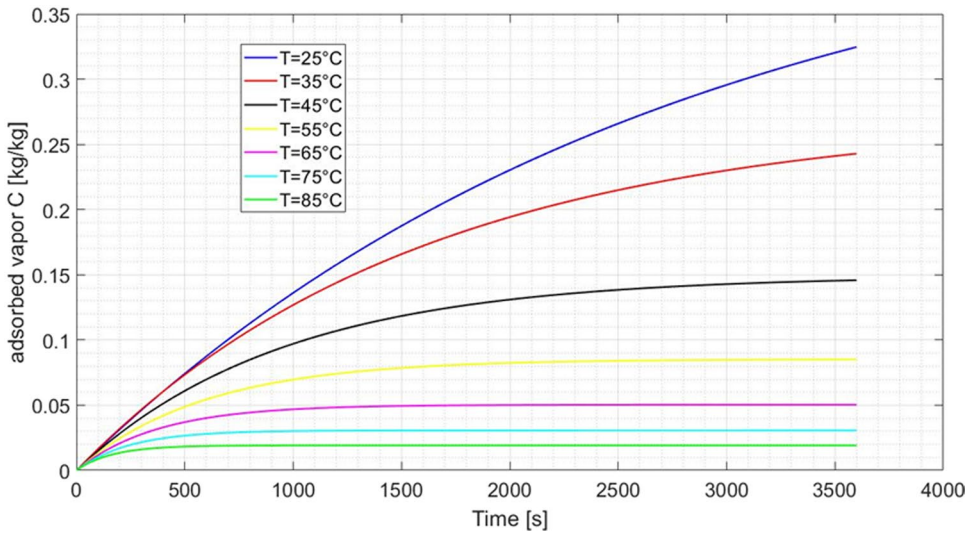

Fig. 4 Silica gel isotherms Fuji RD 2560–Adsorption–half-cycle

based on Eqs. (1), (2), (3), and (4) at a time of 1 h (3,600 s), corresponding to half a cycle, for different temperature ranges varying between 25 and 85 °C.

The initial evaluation of the adsorption kinetics between silica gel and water characterizes the material's behavior under various operating temperatures and enables assistance in determining optimal operating cycle times to maximize the difference between the amounts of adsorbed and desorbed vapor in each cycle. The greater these differences, the better the SDWP, SCP, and COP performance indices will be. The theoretical determination of the optimum cycle time relies on the system configuration and the pre-adjustment of operational parameters such as the maximum temperature of the thermal source used in desorption, the minimum temperature available for use in the adsorption process, operating pressures, and the saline concentration of the feed source. In the case of temporal variability for some or several of these parameters, there will also be variability in the optimal cycle time depending on the set of parameters used.

The main objective of this work is to evaluate the performance of an adsorption desalination system considering the transient nature of ambient temperature and the consequent changes in the reservoir temperature due to the variability of the global horizontal radiation index over a typical day. Thus, the half-cycle time adopted in the simulations is 1 h (3,600 s). Additionally, within this same time interval, ambient temperature and global horizontal irradiance data provided by the meteorological station were collected and used in this simulation. In this simulation, it is also assumed that the low-temperature thermal fluid flows used in the

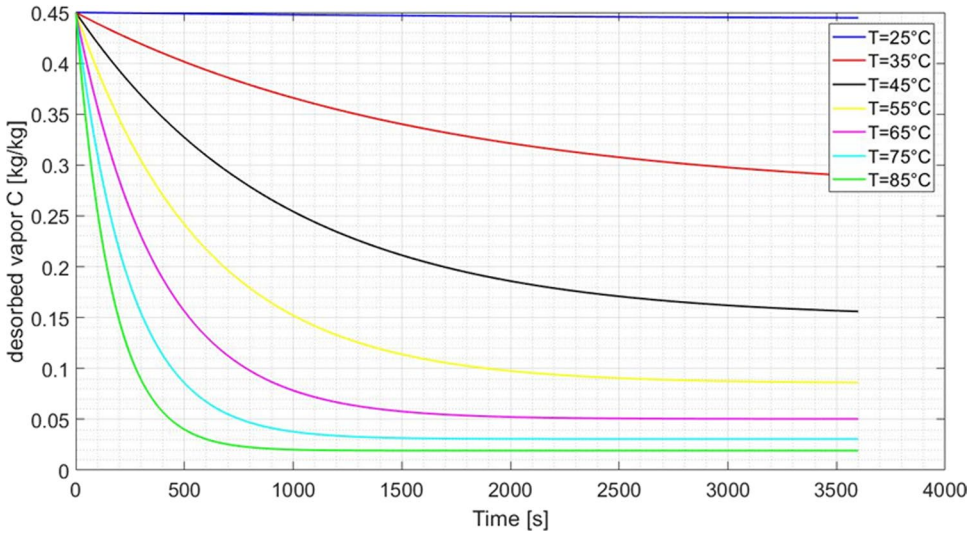

Fig.5 Silica gel isotherms Fuji RD 2560–Desorption–half-cycle

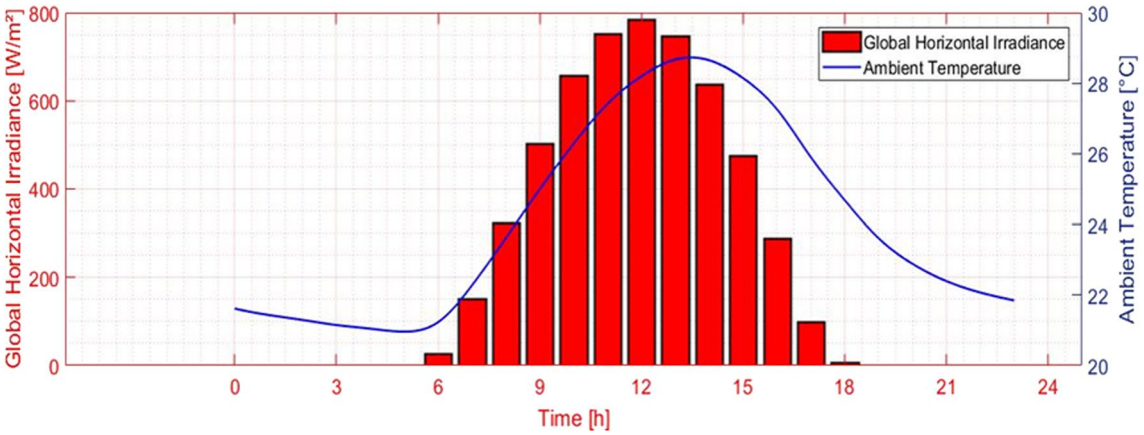

Fig.6 The average values of global horizontal irradiance (I_c) and ambient temperature (T_{amb}) for a typical day

evaporator ($T_{chil,in}$), adsorptive reactors ($T_{cw,in}$), and condenser ($T_{wcond,in}$) originate from the same reservoir, which takes on the variations in ambient temperature (T_{amb}). Similarly, the high-temperature thermal ($T_{hw,in}$) source, neglecting thermal losses through the connecting pipes, assumes the same temperature as the collector reservoir (T_s). Figure 6 presents variations in the average values of T_{amb} and I_c over a typical day, which were derived from data collected by a meteorological station located in Campina Grande, a city in the semiarid region in Brazil. It can be observed that solar radiation is zero during the night and gradually increases throughout the solar day from 6:00 to 18:00 h, reaching a maximum average value of 780 W/m^2. Similarly, the ambient temperature during this same period of the day reaches a maximum average value of 29 °C.

Figure 7 presents the temperature transient of the thermal reservoir (T_s) as a function of the variation in the global horizontal irradiance radiation (I_c) over a representative day. It can be observed that starting at 6:00 h, the solar collector's reservoir begins its heating process, reaching a maximum temperature of 74 °C at 15:00 h. In a previously published work by (Mitra et al. 2017), it was determined that for an adsorptive system using the silica gel and water pair, the theoretical minimum temperature for the desorption process lies between the values of 48 and 68 °C. This limits the total operation time of the system. In this case, and according to the initial parameters adopted for the simulation of this model, these temperatures are only available within the system between 11:00 and 19:00 h, as illustrated in Fig. 7. Before this period, all the energy from the solar heating system was being used to heat the volume of water contained in the solar collector's reservoir.

The profile of the adsorption and desorption processes as a function of variations in ambient temperatures (T_{amb}) and reservoir temperatures (T_s) occurring in reactors 1 and 2 is illustrated in Fig. 8. It can be observed that the amplitude

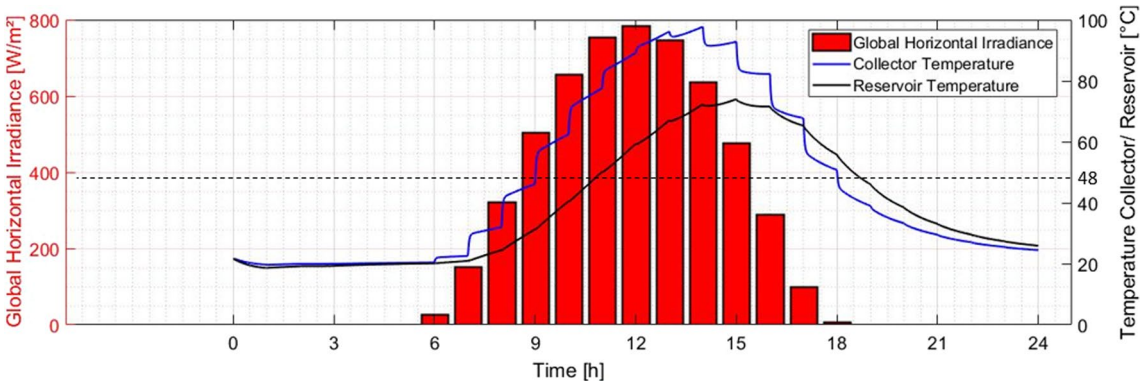

Fig.7 Variation of collector temperature (T_c) and reservoir temperature (T_s) throughout a typical day. Dotted line represents minimum temperature for desorption

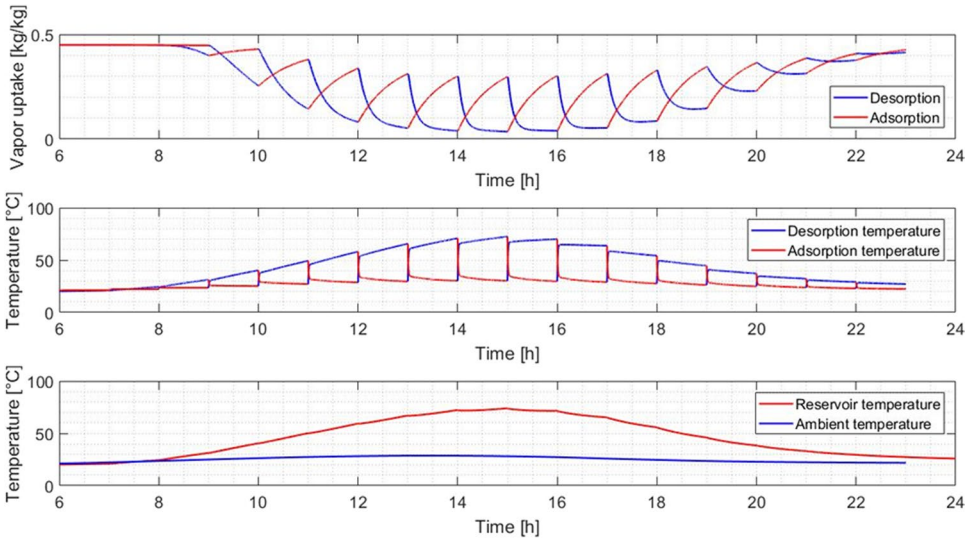

Fig.8 **a** Adsorptive cycle reactors 1 and 2, **b** Temperature variation during adsorption/desorption, **c** Reservoir temperature/ambient temperature variation

between the curves of these two processes represents the amount of vapor released per cycle from each reactor to the condenser. The highest value of 0.25 kg/kg per cycle is obtained between the period of 14:00 to 16:00 h coinciding with the period of the day with the greatest thermal amplitude (40 °C). It is notable that between 10:00 and 20:00 h, the system remains productive even after the global radiation index drops to zero after 18:00 h due to the availability of residual thermal energy in the solar collector's reservoir.

Figure 9a, b illustrates the dynamics of temperature profiles for the adsorptive cycle obtained from the simulation of the current model for the evaporator, adsorptive reactors, and condenser. In Fig. 9a, temperature variations are shown for each half-cycle (3,600 s) over a representative day, while in Fig. 9b, these temperature profiles are presented in more detail for the period corresponding to a complete cycle between 14:00 and 16:00 h. The desorption temperature profile in the reactors follows an ascending heating trend until reaching its peak of 74 °C at 15:00 h after which it transitions to a descending cooling profile until it reaches ambient temperature. The refrigeration effect is observed through the evaluation of the temperature profile, $T_{\text{chil,out}}$ in the evaporator. This effect becomes noticeable starting from 10:00 h, reaching a temperature of 15 °C and an SCP of 170 W/kg. Throughout the period between 12:00 and 19:00 h, temperature troughs below 10 °C and SCP values between 280 and 315 W/kg were observed, as illustrated in Fig. 10.

The coefficient of performance (COP) is another relevant performance indicator evaluated in this study. Figure 11 and Fig. 12 present the simulation results of the model according to Eq. (20). Figure 11 shows the variations of the COP for a half-cycle period equivalent to 1 h (3,600 s) for a representative day, and Fig. 12 provides a more detailed view of the period from 14:00 to 16:00 h. It can be observed that at the beginning of the cycle, the COP starts with very low values and increases as the refrigeration effect is generated in the evaporator. The temperature

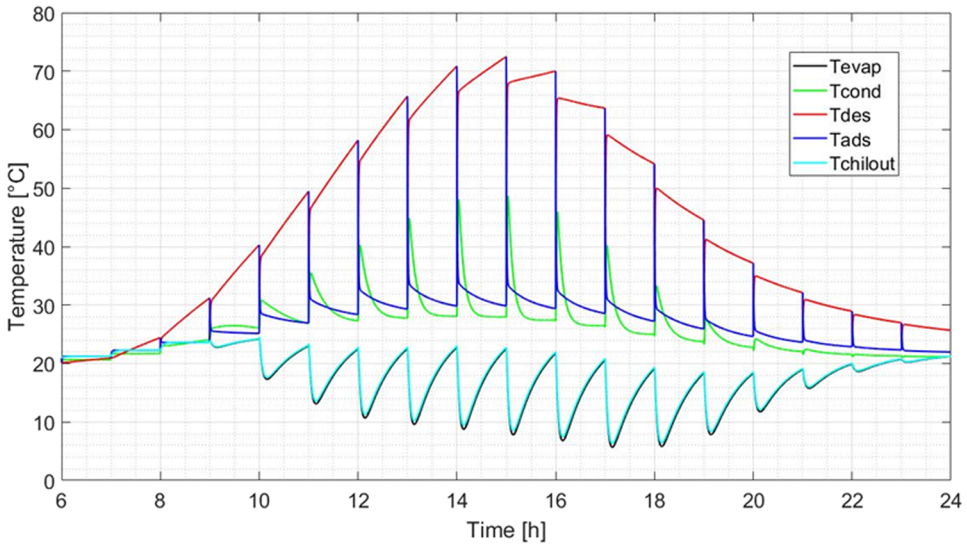

(a)

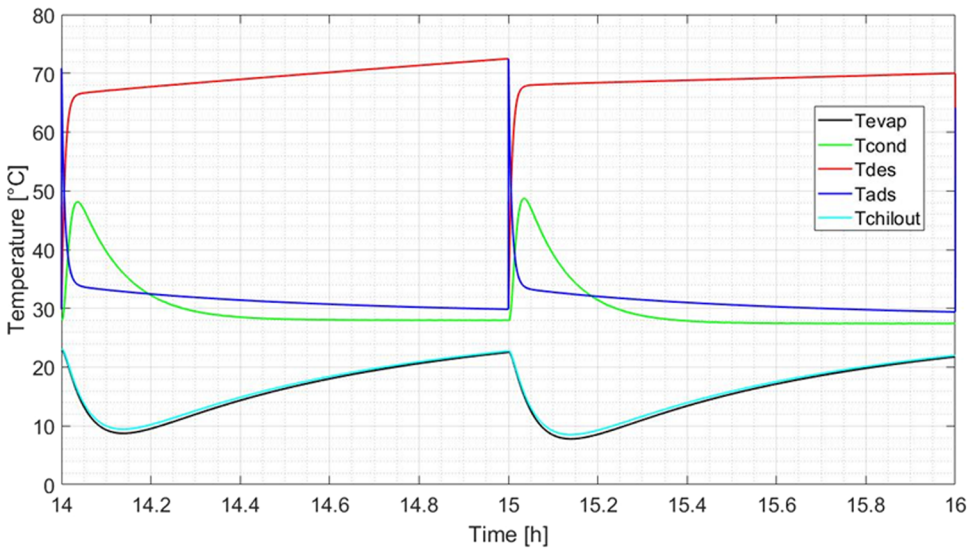

(b)

Fig.9 Temperature profiles in the components of the adsorptive system (SADCS) from 6:00 to 24:00 h in (**a**) and from 14:00 to 16:00 h in (**b**)

drop is more pronounced in the first 600 s, after which the evaporator temperature gradually increases until reaching thermal equilibrium with $T_{chil,in} = T_{amb}$, as illustrated in Fig. 9b. For convenient and comparative purposes, an average COP for this system calculated for a typical day is 0.46, as illustrated in Fig. 13.

Hereafter, in Table 5, the main results of previous experimental studies conducted by other authors, in which ADC systems loaded with silica gel adsorbent are evaluated under various operational conditions and arrangements, are summarized. Additionally, the results of the numerical simulation of this model for comparative purposes are also presented.

To evaluate the influence of feed flow rates for the thermal baths and the number of collectors used on the SDWP system productivity index, the model was subjected to variations in the parameters $\dot{m}_{h/c\,w}$ (reactors) as per Eq. (13) and $\dot{m}_{w,cond}$ (condenser) as per Eq. (10). To minimize computational effort, the simulation values of flow rates were assigned equally to both parameters between 0.1 and 0.9 kg/s.

In Fig. 14, it can be observed that for this model, the SDWP productivity index is not highly sensitive to the increase in the thermal bath feeding capacity for flow rates above 0.4 kg/s. Additionally, an increase in capacity would result in higher power demands for the pumping system and increased system pressure losses. Each collector used in this simulation has an area $A_c = 4.46\ m^2$. Analyzing Fig. 14, it can be seen that for each adopted thermal bath flow rate, the

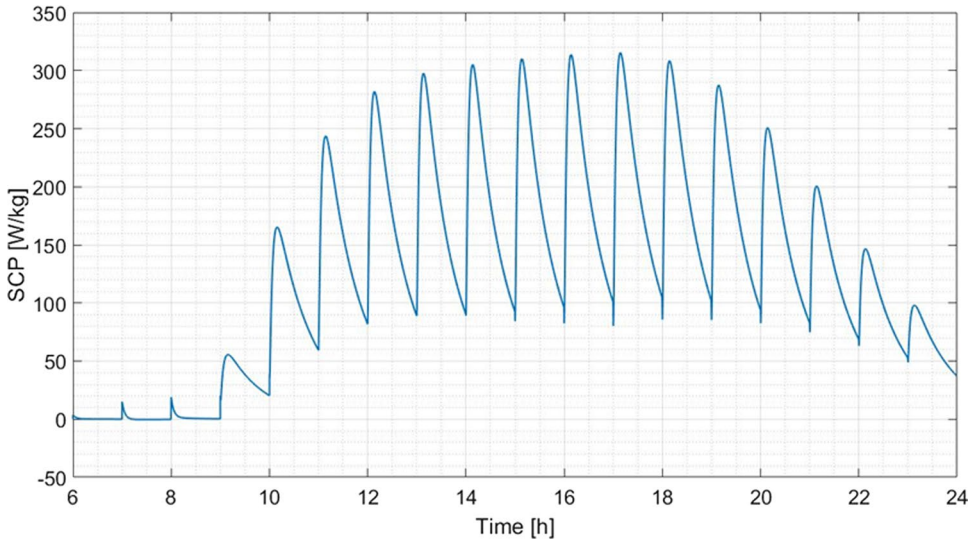

Fig.10 Specific cooling power (SCP) performance indicator on a typical day

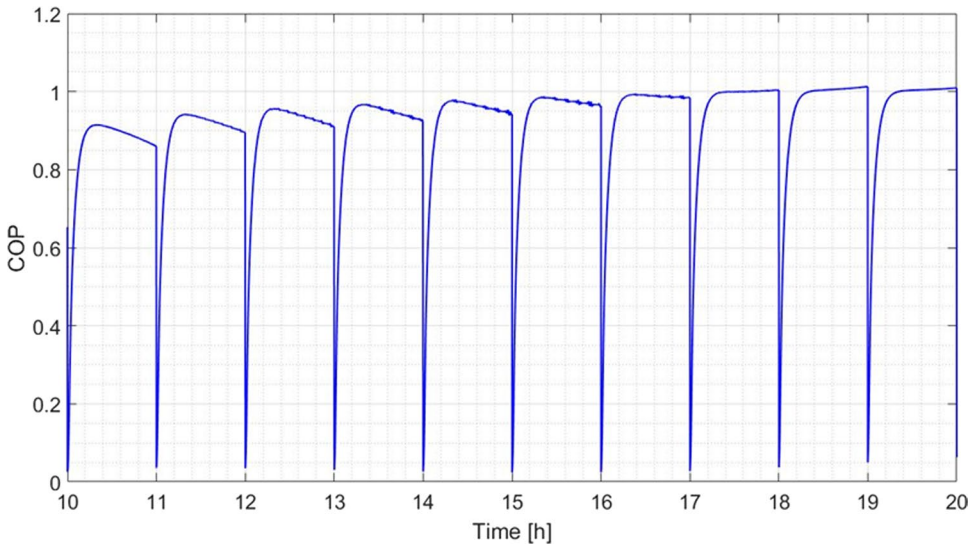

Fig.11 Evolution of COP for the half-cycles throughout a typical day

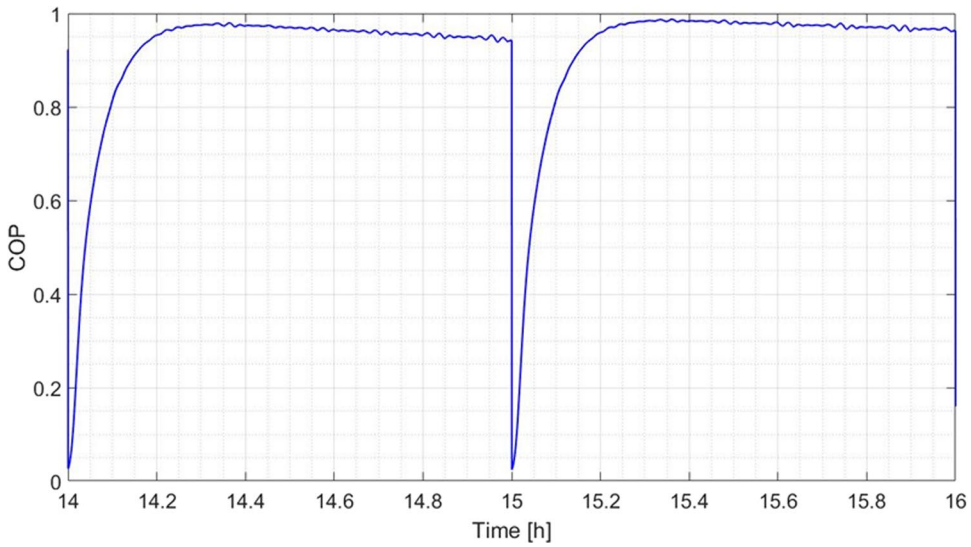

Fig.12 COP variation during the period from 14:00 to 16:00 h on a typical day

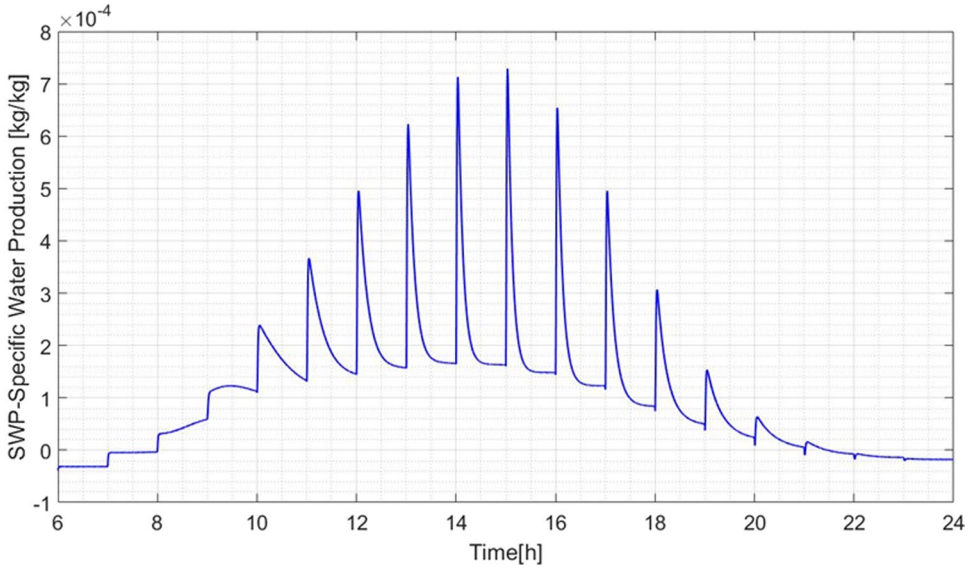

Fig.13 SWP profile over a typical day

Table 5 Summary of previous experimental tests of ADC systems with silica gel

Half-cycle time (s)	N° bed	Adsorbent weight (kg)	Tcw (°C)	Thw (°C)	SDWP (m^3/ton)	SCP (W/kg)	COP	REF
180	4	36	30	85	4.7	–	0.28	(Wang and Ng 2005)
650	2	6.75	30	85	4	112	0.45	(Alsaman et al. 2017)
600	4	36	30	85	14.2	–	0,74	(Thu et al. 2011)
900	2	29.17	27	83	4.69	–	0.766	(Zhang et al. 2020)
600	4/2	36	30	85	10	–	0.61	(Thu et al. 2009)
480	4	36	29.5	85	8	181	–	(Ng et al. 2012)
3600	2	7	21–29	48–68	6.26	5–300	0.46	current work

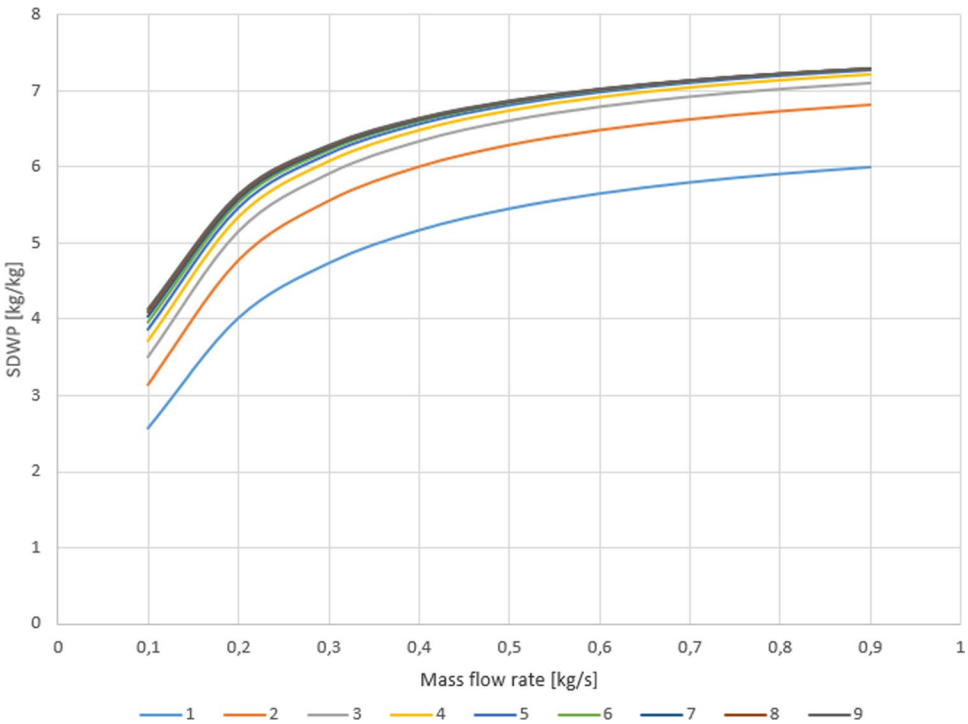

Fig.14 Influence of flow rate and the number of collectors on the productivity of potable water SDWP

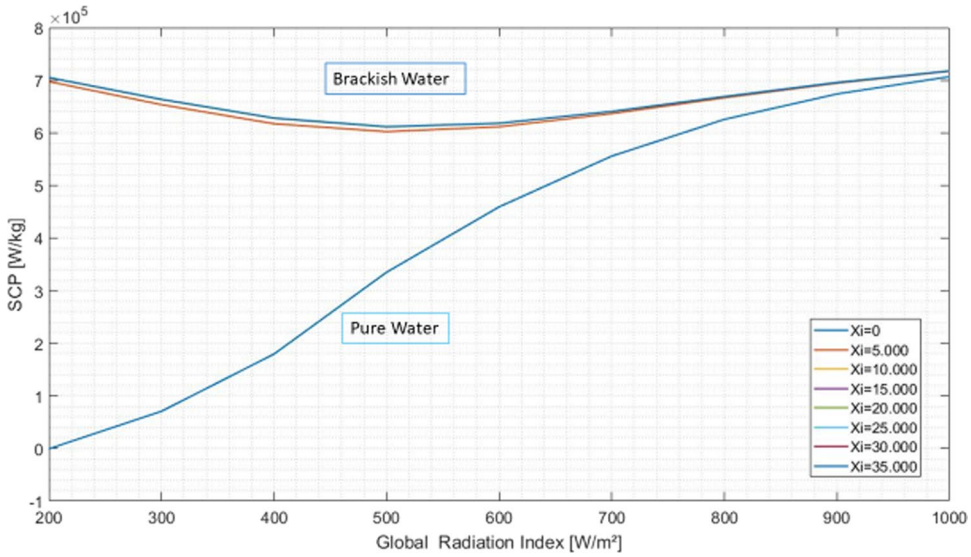

Fig.15 Variation of SCP as a function of global radiation index and salinity level

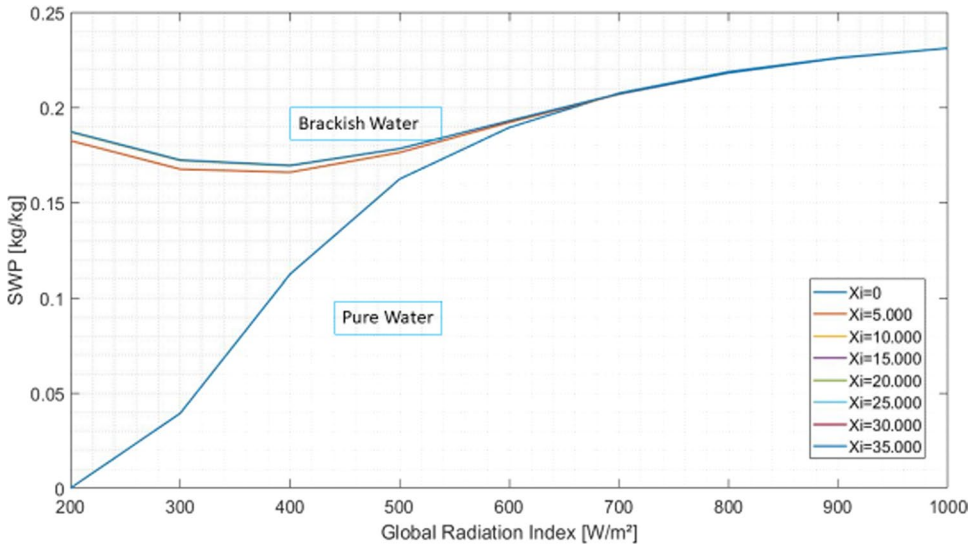

Fig.16 Variation of SWP as a function of global radiation index and salinity level

system's productivity shows minimal variation for systems equipped with more than three solar collectors.

The global horizontal irradiance indices (I_c) and salinity concentration (χ_i) of the groundwater source here are input parameters for the evaluated model (SADCS) and are subject to variations throughout a typical day, as well as seasonal changes and shifts in rainfall patterns. Figure 15 and Fig. 16 illustrate the impact of these parameter variations on the SCP and SWP performance indices. Salinity concentrations were evaluated ranging from 0 ppm (χ_i=0, for pure water) to 35,000 ppm (χ_i=35,000 for seawater), and from 200 to 1,000 W/m^2 for the global horizontal irradiance index (I_c). In both cases, it is observed that, within the range of salinity for the evaluated brackish water, the performance index shows little sensitivity as can be observed in Fig. 15 and Fig. 16 through the overlap of curves from different evaluated salt concentrations. In the theoretical and experimental work by Bai et al. (Bai et al. 2020), they assessed the influence of salinity on the performance of an adsorption desalination system, and the results did not show significant changes in the SWP index for samples ranging from 35,000 to 100,000 ppm. Starting from 750 W/m^2, as shown in the figure, brackish water essentially performs similarly to pure water. The influence of salinity on the system is most pronounced in the evaporator, affecting the amount of heat required to maintain the evaporative process as salinity concentration increases, thereby raising the boiling point elevation (BPE) and reducing the latent heat of vaporization (Sharqawy et al. 2010).

According to the work of Spiegler and El-Sayed (2001) and Ng et al. (2013), the ideal work for desalination, as indicated by the approach of work done and Gibbs free

energy, has been shown to be sensitive to the saline concentration of the feed water. For instance, the theoretical minimum energy required to desalinate standard seawater feed with a concentration of 35,000 ppm is 0.706 kWh/m^3. This thermodynamic limit is independent of the desalination method employed. From the perspective of energy efficiency and environmental sustainability, there is a strong motivation for engineers and researchers to enhance the specific energy consumption in the desalination process. Currently, due to technological advancements in new materials applied to membranes, as well as the adoption of energy recovery processes, the specific energy consumption (SEC) has been reduced to 30% of the average consumption of 6 kWh/m^3 for desalination of standard seawater. Although SEC is commonly used as a performance indicator, it lacks the ability to discern between energy forms incurring costs and those that do not, when employed as inputs in processes. Additionally, it can be applied to assess and compare processes fueled by either electrical or thermal energy sources. The combination of these two forms of energy constitutes the primary energy input, and according to Ng et al. (2013), the values can reach 14.29 kWh/m^3 for reverse osmosis (RO) processes and 39.80 kWh/m^3 for adsorption desalination (AD) processes. Nevertheless, the electricity consumption for these processes amounts to 5 and 1.38 kWh/m^3, respectively. As the main components of the adsorption desalination system are stationary, the low electrical consumption is related to the operation of fluid transfer and vacuum pumps, actuation of valves, instrumentation, and control panel, a load that can be met by the addition of photovoltaic panels and small batteries to the system. The addition of batteries to the system not only supports peripheral systems but also helps extend the operating period of the system after a reduction in solar irradiation levels by powering electric resistances installed in adsorptive reactors, ensuring minimum temperatures for the maintenance of the adsorptive cycle and improving SDWP indices.

Conclusions

This study has undertaken a thorough evaluation of the viability of employing non-concentrated solar thermal energy-activated adsorption technology in the context of desalination processes. It involved the development of a sophisticated mathematical model and the integration of meteorological data and groundwater salinity data from the semiarid northeastern region of Brazil. Through this analysis, the complex interplay between meteorological conditions, salinity fluctuations, and the performance of the system was assessed.

The conducted numerical analyses have shed light on the transient temperature variations resulting from climatic shifts, as well as the influence of salinity changes in underground water sources on the suggested model's performance indicators. By evaluating operational parameters, including the feed flow rate of thermal baths within reactors and condensers, insights into the system's efficiency in terms of specific daily water production (SDWP) were gained, considering the optimal deployment of solar collectors.

The implications of diverse global radiation indices during periods of sunlight exposure on both ambient temperature and the temperature of the solar collector reservoir have indicated an SDWP spanning from 1 to 9 kg/kg. Notably, this includes an aggregated value of 6.26 kg/kg (SDWP) over a typical day. Furthermore, the assessment of the cooling effect under varying ambient temperatures has highlighted a range of 50 to 300 W/kg for the specific cooling power (SCP), culminating in temperatures dipping below 10 °C during the characteristic daily cycle. Groundwater sources in the Brazilian semiarid region predominantly exhibit brackish waters with salinity indices ranging from 0 to 15,000 ppm. The model demonstrated limited sensitivity in terms of SDWP and SCP performance indices within this lower salinity range.

Considering an average per capita consumption of 150 l/day and a family's estimated daily usage of 600 l/day, the model recommends a desalination setup utilizing adsorption with 90 kg of adsorbent material (silica gel). This allocation is distributed across two reactors and four solar collectors, collectively covering an area of 18 m^2 within the solar field. These findings stand in alignment with comparable theoretical and experimental works documented in the literature, affirming the promising potential of this technology as a viable alternative to conventional reverse osmosis processes.

As the global pursuit of sustainable and effective water treatment methodologies advances, the insights gleaned from this study provide valuable direction for the innovation and implementation of novel desalination systems. By bridging the gap between renewable energy utilization and water resource management, these findings contribute significantly to the ongoing evolution of solar-driven desalination technologies. The robustness demonstrated within the context of the semiarid Northeastern Brazilian region underscores the adaptability and resilience of this approach. This study serves as a foundation for further exploration and optimization of these systems across diverse geographical and climatic contexts.

Acknowledgements The first author acknowledges the financial support received from FAP-DF (Fundação de Amparo a Pesquisa do Distrito Federal, Brazil) TOA 178/2021, under the Mobility Confap Italy - MCI 2019 program.

Authors contributions RM contributed to conceptualization, literature review, investigation, formal analysis, writing and editing the original draft, and MS contributed to methodology, supervision, review, and editing.

Funding The author(s) received no specific funding for this work.

Data availability The data supporting this study's findings are available from the corresponding author upon reasonable request.

Declarations

Conflict of interest The authors have no competing interests to declare that are relevant to the content of this article.

References

Alam KCA, Saha BB, Kang YT et al (2000) Heat exchanger design effect on the system performance of silica gel adsorption refrigeration systems. Int J Heat Mass Transf 43:4419–4431. https://doi.org/10.1016/S0017-9310(00)00072-7

Ali SM, Chakraborty A (2016) Adsorption assisted double stage cooling and desalination employing silica gel + water and AQSOA-Z02+water systems. Energy Convers Manag 117:193–205. https://doi.org/10.1016/j.enconman.2016.03.007

Ali ES, Harby K, Askalany AA et al (2017) Weather effect on a solar powered hybrid adsorption desalination-cooling system: A case study of Egypt's climate. Appl Therm Eng 124:663–672. https://doi.org/10.1016/j.applthermaleng.2017.06.048

Ali ES, Alsaman AS, Tawfik MHM et al (2024a) Solar-powered hybrid adsorption desalination/humidification-dehumidification system. Therm Sci Eng Prog 51:102598. https://doi.org/10.1016/J.TSEP.2024.102598

Ali ES, Harby K, Alsaman AS (2024b) New and effective combination of an absorption desalination systems with adsorption and humidification-dehumidification desalination systems utilizing internal heat recovery methods. Desalination 583:117657. https://doi.org/10.1016/J.DESAL.2024.117657

Alsaman AS, Askalany AA, Harby K, Ahmed MS (2017) Performance evaluation of a solar-driven adsorption desalination-cooling system. Energy 128:196–207. https://doi.org/10.1016/j.energy.2017.04.010

Alsaman AS, Ghazy M, Ali ES et al (2024) Solar-powered adsorption desalination utilizing composite silica gel with a humidification-dehumidification desalination system. Desalination 582:117663. https://doi.org/10.1016/J.DESAL.2024.117663

Aristov YI, Tokarev MM, Freni A et al (2006) Kinetics of water adsorption on silica Fuji Davison RD. Microporous Mesoporous Mater 96:65–71. https://doi.org/10.1016/j.micromeso.2006.06.008

Askalany A, Alsaman AS, Ghazy M et al (2021) Experimental optimization of the cycle time and switching time of a metal organic framework adsorption desalination cycle. Energy Convers Manag 245:114558. https://doi.org/10.1016/j.enconman.2021.114558

Bai S, Ho TC, Ha J et al (2020) Study of the salinity effects on the cooling and desalination performance of an adsorption cooling cum desalination system with a novel composite adsorbent. Appl Therm Eng 181:115879. https://doi.org/10.1016/j.applthermaleng.2020.115879

Brazil (2010) Programa Água Doce. Base Document [portuguese].2010. Avaiable at:http://www.aesa.pb.gov.br/aesa-website/wp-content/uploads/2016/11/doc_PAD_01.pdf

Buzás J, Farkas I, Biró A, Németh R (1998) Modelling and simulation of a solar thermal system. Math Comput Simul 48:33–46. https://doi.org/10.1016/s0378-4754(98)00153-0

Buzás J (2009) Block-Oriented Modeling of Solar Thermal

Chihara K, Suzuki M (1983) Air drying by pressure swing adsorption. J Chem Eng Japan 16:293–299. https://doi.org/10.1252/jcej.16.293

Chua HT, Ng KC, Chakraborty A et al (2002a) Adsorption characteristics of silica gel + water systems. J Chem Eng Data 47:1177–1181. https://doi.org/10.1021/je0255067

Chua HT, Ng KC, Chakraborty A et al (2002b) Adsorption characteristics of silica {gel}+water {systems}. J Chem Eng Data Chem Eng 47:1177–1181

Elsayed E, AL-Dadah R, Mahmoud S, et al (2017) CPO-27(Ni), aluminium fumarate and MIL-101(Cr) MOF materials for adsorption water desalination. Desalination 406:25–36. https://doi.org/10.1016/j.desal.2016.07.030

Elsayed E et al (2020) Experimental testing of aluminium fumarate MOF for adsorption desalination. Desalination 475:114170. https://doi.org/10.1016/j.desal.2019.114170

Ferreira RS, Veiga HP, dos Santos RG, Saia A, Rodrigues SC, Bezerra AF, Hermes LC, Moura A, Cunha LH. Empowering Brazilian Northeast rural communities to desalinated drinking water access: Programa Água Doce. In: The International Desalination Association World Congress, 2017, São Paulo. Water reuse and desalination ensure your water future.São Paulo: International Desalination Association, 2017

Gado MG, Ookawara S, Nada S et al (2024) Adsorbent beds packed in triply periodic minimal surface-derived structures and their performance in adsorption desalination/cooling systems. Int Commun Heat Mass Transf 150:107205. https://doi.org/10.1016/j.icheatmasstransfer.2023.107205

Goldsworthy MJ (2014) Measurements of water vapour sorption isotherms for RD silica gel, AQSOA-Z01, AQSOA-Z02, AQSOA-Z05 and CECA zeolite 3A. Microporous Mesoporous Mater 196:59–67. https://doi.org/10.1016/j.micromeso.2014.04.046

Han B, Chakraborty A (2022) Highly efficient adsorption desalination employing protonated-amino-functionalized MOFs. Desalination 541:116045. https://doi.org/10.1016/j.desal.2022.116045

International Desalination and Reuse Association (2019) IDRA water security handbook 2019–2020

Kakaç S, Liu H, Pramuanjaroenkij A (2012) Heat exchanger selection and design. Third Edit. CRC Press - Talor & Francis Group, Boca Raton -FL

Kicsiny R, Varga Z (2012) Real-time state observer design for solar thermal heating systems. Appl Math Comput 218:11558–11569. https://doi.org/10.1016/j.amc.2012.05.040

Kumar R, Rosen MA (2010) Thermal performance of integrated collector storage solar water heater with corrugated absorber surface. Appl Therm Eng 30:1764–1768. https://doi.org/10.1016/j.applthermaleng.2010.04.007

Li M, Zhao Y, Long R et al (2021) Field synergy analysis for heat and mass transfer characteristics in adsorption-based desalination and cooling systems. Desalination 517:115244. https://doi.org/10.1016/j.desal.2021.115244

Liu YM, Yuan ZX, Wen X, Du CX (2021) Evaluation on performance of solar adsorption cooling of silica gel and SAPO-34 zeolite.

Appl Therm Eng 182:116019. https://doi.org/10.1016/j.applthermaleng.2020.116019
Mitra S, Srinivasan K, Kumar P et al (2014) Solar driven adsorption desalination system. Energy Procedia 49:2261–2269. https://doi.org/10.1016/j.egypro.2014.03.239
Mitra S, Thu K, Saha BB, Dutta P (2017) Performance evaluation and determination of minimum desorption temperature of a two-stage air cooled silica gel/water adsorption system. Appl Energy 206:507–518. https://doi.org/10.1016/j.apenergy.2017.08.198
Myat A, Kim Choon N, Thu K, Kim YD (2013) Experimental investigation on the optimal performance of Zeolite-water adsorption chiller. Appl Energy 102:582–590. https://doi.org/10.1016/j.apenergy.2012.08.005
Nayar KG, Sharqawy MH, Banchik LD, Lienhard JH (2016) Thermophysical properties of seawater: A review and new correlations that include pressure dependence. Desalination 390:1–24. https://doi.org/10.1016/j.desal.2016.02.024
Ng KC, Chua HT, Chung CY et al (2001) Experimental investigation of the silica gel-water adsorption isotherm characteristics. Appl Therm Eng 21:1631–1642. https://doi.org/10.1016/S1359-4311(01)00039-4
Ng KC, Thu K, Chakraborty A et al (2009) Solar-assisted dual-effect adsorption cycle for the production of cooling effect and potable water. Int J Low-Carbon Technol 4:61–67. https://doi.org/10.1093/ijlct/ctp008
Ng KC, Thu K, Saha BB, Chakraborty A (2012) Study on a waste heat-driven adsorption cooling cum desalination cycle. Int J Refrig 35:685–693. https://doi.org/10.1016/j.ijrefrig.2011.01.008
Ng KC, Thu K, Kim Y et al (2013) Adsorption desalination: An emerging low-cost thermal desalination method. Desalination 308:161–179. https://doi.org/10.1016/j.desal.2012.07.030
Olkis C, Al-Hasni S, Brandani S et al (2021) Solar Powered Adsorption Desalination for Northern and Southern Europe. Energy 232:120942. https://doi.org/10.1016/j.energy.2021.120942
Pakere I, Lauka D, Blumberga D (2018) Solar power and heat production via photovoltaic thermal panels for district heating and industrial plant. Energy 154:424–432. https://doi.org/10.1016/j.energy.2018.04.138
Rezk H, Alsaman AS, Al-Dhaifallah M et al (2019) Identifying optimal operating conditions of solar-driven silica gel based adsorption desalination cooling system via modern optimization. Sol Energy 181:475–489. https://doi.org/10.1016/j.solener.2019.02.024
Ruthven DM (2008) Fundamentals of adsorption equilibrium and kinetics in microporous solids. Mol Sieves - Sci Technol 7:1–43. https://doi.org/10.1007/3829_007
Sakoda A, Suzuki M (1984) Fundamental study on solar powered adsorption cooling system. J Chem Eng Japan 17:52–57. https://doi.org/10.1252/jcej.17.52
Sharqawy MH, Lienhard VJH, Zubair SM (2010) Thermophysical properties of seawater: a review of existing correlations and data. Desalin Water Treat 16:354–380. https://doi.org/10.5004/dwt.2010.1079
Spiegler KS, El-Sayed YM (2001) The energetics of desalination processes. Desalination 134:109–128. https://doi.org/10.1016/S0011-9164(01)00121-7
Thu K, Ng KC, Saha BB et al (2009) Operational strategy of adsorption desalination systems. Int J Heat Mass Transf 52:1811–1816. https://doi.org/10.1016/j.ijheatmasstransfer.2008.10.012
Thu K, Saha BB, Chakraborty A et al (2011) Study on an advanced adsorption desalination cycle with evaporator-condenser heat recovery circuit. Int J Heat Mass Transf 54:43–51. https://doi.org/10.1016/j.ijheatmasstransfer.2010.09.065
Thu K, Chakraborty A, Kim YD et al (2013a) Numerical simulation and performance investigation of an advanced adsorption desalination cycle. Desalination 308:209–218. https://doi.org/10.1016/j.desal.2012.04.021
Thu K, Chakraborty A, Saha BB, Ng KC (2013b) Thermo-physical properties of silica gel for adsorption desalination cycle. Appl Therm Eng 50:1596–1602. https://doi.org/10.1016/j.applthermaleng.2011.09.038
Velte-Schäfer A, Laurenz E, Füldner G (2023) Basic adsorption heat exchanger theory for performance prediction of adsorption heat pumps. iScience 26(12):108432. https://doi.org/10.1016/j.isci.2023.108432
Vivekh P, Kumja M, Bui DT, Chua KJ (2018) Recent developments in solid desiccant coated heat exchangers—a review. Appl Energy 229:778–803. https://doi.org/10.1016/j.apenergy.2018.08.041
Wang X, Ng KC (2005) Experimental investigation of an adsorption desalination plant using low-temperature waste heat. Appl Therm Eng 25:2780–2789. https://doi.org/10.1016/j.applthermaleng.2005.02.011
Wibowo E, Sutisna RM et al (2017) Utilization of Natural Zeolite as Sorbent Material for Seawater Desalination. Procedia Eng 170:8–13. https://doi.org/10.1016/j.proeng.2017.03.002
Wu JW, Biggs MJ, Hu EJ (2010) Thermodynamic analysis of an adsorption-based desalination cycle. Chem Eng Res Des 88:1541–1547. https://doi.org/10.1016/j.cherd.2010.04.004
Wu JW, Biggs MJ, Pendleton P et al (2012) Experimental implementation and validation of thermodynamic cycles of adsorption-based desalination. Appl Energy 98:190–197. https://doi.org/10.1016/j.apenergy.2012.03.022
Youssef PG, Al-Dadah RK, Mahmoud SM et al (2015a) Effect of evaporator and condenser temperatures on the performance of adsorption desalination cooling cycle. Energy Procedia 75:1464–1469. https://doi.org/10.1016/j.egypro.2015.07.263
Youssef PG, Mahmoud SM, AL-Dadah RK (2015b) Performance analysis of four bed adsorption water desalination/refrigeration system, comparison of AQSOA-Z02 to silica-gel. Desalination 375:100–107. https://doi.org/10.1016/j.desal.2015.08.002
Youssef PG, Mahmoud SM, AL-Dadah RK (2016) Numerical simulation of combined adsorption desalination and cooling cycles with integrated evaporator/condenser. Desalination 392:14–24. https://doi.org/10.1016/j.desal.2016.04.011
Zhang H, Ma H, Liu S et al (2020) Investigation on the operating characteristics of a pilot-scale adsorption desalination system. Desalination 473:114196. https://doi.org/10.1016/j.desal.2019.114196